Decoupling of a Wideband Dual-Polarized Large-Scale Antenna Array with Dielectric Stubs

Mei, Peng; Zhang, Yiming; Zhang, Shuai

Published in:
I E E E Transactions on Vehicular Technology

DOI (link to publication from Publisher):
10.1109/TVT.2021.3089832

Publication date:
2021

Document Version
Accepted author manuscript, peer reviewed version

Decoupling of a Wideband Dual-Polarized Large-Scale Antenna Array with Dielectric Stubs

Peng Mei, *Student Member, IEEE*, Yi-Ming Zhang, *Member, IEEE*, and Shuai Zhang, *Senior Member, IEEE*

***Abstract*— A technique of decoupling dielectric stubs (DDS) is proposed for mutual coupling reduction of wideband, dual-polarized, and large-scale antenna arrays in this paper, where a low dielectric constant DDS is mounting on a dual-polarized and wideband antenna array seamlessly. The decoupling mechanism of the proposed DDS is qualitatively explained. By properly optimizing the dielectric constant and dimensions of the dielectric stubs, the DDS can reduce the mutual couplings between array elements efficiently. The dielectric stubs are considered as perturbations to slightly localize the electromagnetic fields radiated from the antenna element to lower the space wave coupling. The advantages of the proposed decoupling technique are wideband, low cost, high efficiency, and suitable for large-scale antenna arrays. For demonstration, 4 × 4 dual-polarized and wideband antenna arrays with and without the DDS are simulated, measured, and compared. The simulated results show that the antenna array with the DDS can achieve all port-to-port isolations over 25 dB from 4.4 to 5.0 GHz for all the coupling paths, which are 7 dB higher than the counterparts without the DDS. Moreover, the total efficiencies of the antenna elements with the proposed DDS are also improved. The measured results agree well with the simulated, verifying the effectiveness of the proposed method of DDS for decoupling of large-scale antenna arrays.**

***Index Terms*— Mutual coupling, broadband, dual-polarization, array antenna, massive MIMO, dielectric stub.**

I. Introduction

Multiple-input multiple-output (MIMO) is served as an indispensable technology since it has been proved to significantly enhance spectrum efficiency and channel capacity [1]-[5]. Strong mutual coupling between MIMO antenna elements will degrade the MIMO performance. Typically, the isolation of 15-17 dB is already enough to satisfy the requirements of MIMO channel capacity or error rate [5]. Massive MIMO is well known as one of the key technologies for 5G wireless communications. Massive MIMO can further increase the MIMO channel capacity by exploiting the directivity and beam steering of large-scale MIMO antenna arrays. The focused and steerable beam of a massive MIMO antenna array allows it to accurately track individual users, which can be used in wireless communications between MIMO base station and vehicles as shown in Fig.1. to offer a better and reliable connection. Besides the MIMO performance, the mutual coupling in massive MIMO would also distort the active VSWR of the antenna elements in a large-scale antenna array and the efficiencies of the power amplifiers [5]. Moreover, the inter-element coupling also impacts the radiation patterns of the antenna elements in an array and the gain-loss at a large scanning angle. Therefore, isolation enhancement between massive MIMO array elements is highly desired, and the mutual coupling of below -25 dB is recommended or required in the industry.

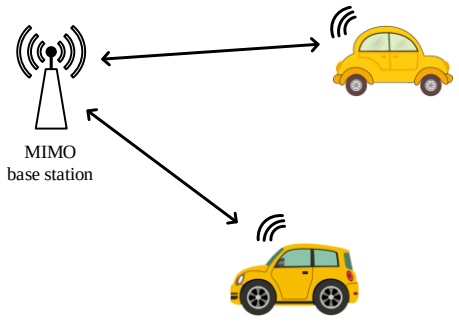

Fig.1. Application scenario of wireless communications between MIMO base station and vehicles.

In general, mutual couplings between antenna elements happen in three different electromagnetic wave coupling paths: a). space wave coupling in free space; b). surface wave coupling within the substrate or in the interface of the substrate and free space; c). on-ground current coupling. Weakening part or all of the three coupling paths is the current strategies to reduce mutual couplings between antenna elements. In massive MIMO antenna arrays, the inter-element distance is typically slightly larger than $0.5\lambda_o$, where the coupling path a) (space wave coupling) is the main challenge to realize over 25 dB isolation compared with paths b) and c).

The past decades have witnessed the developments of decoupling technologies. The defected ground structure (DGS) was usually etched on the metal ground to perform band-stop filtering characteristics to prevent the on-ground current couplings from one antenna element to the others for isolation enhancements [6]-[9]. However, the DGSs might increase the

This work was supported in part by AAU Young Talent Program and also in part by Huawei Project of "5G mmWave Decoupling Array". (*Corresponding author: Shuai Zhang*)

The authors are all with the Antennas, Propagation and Millimeter-wave Systems (APMS) section, Department of Electronic Systems, Aalborg University, Aalborg, 9220, Denmark. (email: sz@es.aau.dk)

back radiation, break the ground plane, and have narrow decoupling bandwidth, which is not suitable for decoupling large-scale antenna arrays in a wide band. The electromagnetic bandgap (EBG) structures are also widely used for isolation enhancement between antenna elements by applying the bandstop property to suppress the surface wave coupling. In [10], Yang *et al.*, placed the square-shaped EBG structures between two antenna elements to block the surface wave coupling for isolation enhancement. It was also found the effect of decoupling is more remarkable with the increment of EBG structures. To this end, EBG structures are not suitable for closely packed antenna arrays since they require large areas to accommodate. Other structures like uniplanar compact EBG (UC-EBG), split-ring resonator (SRR), or modified SRR took the same decoupling mechanisms of EBG structures to reduce mutual couplings [11]-[13]. However, the EBG structures can effectively reduce the mutual couplings in a narrow band, which limits their applications. Neutralization line is another highly effective approach to decouple dual-element antenna systems [14]-[17]. By properly designing the neutralization line, it can introduce an extra coupling path to cancel the original space wave coupling paths. However, the decoupling mode of the neutralization line is not easy to excite, especially in a large-scale antenna array.

To reduce the mutual couplings of dual-polarized massive MIMO antenna arrays (4 × 4 or even larger), different techniques have recently been developed. Transmission-line-based decoupling networks have been introduced in [17], [18]. The transmission-line-based decoupling network in [17] can efficiently reduce coupling for a dual-polarized array but gives narrow decoupling bandwidth, high complexity, and a slightly total efficiency drop. The decoupling bandwidth has been significantly improved with transmission-line-based wave trap [18], [19]. However, this method is challenging to apply in dual-polarized arrays due to the high cross-polarization coupling. A decoupling ground (DG) was proposed in [20] to use the on-ground current coupling to cancel the space wave coupling, but the inter-element distance of the array is relatively large to obtain the isolation of 25 dB. Antenna-array decoupling surface (ADS) was recently proposed by Wu *et al* [21]. A surface with certain metal patterns is located above the antenna array to introduce additional reflected waves to cancel the space wave coupling in free space. The decoupling effects of ADS for large-scale and dual-polarized antennas have been improved with phase compensation as reported in [22]. The key for a good ADS is to optimize its reflection phases to make them cope with the phases of the direct couplings to achieve a significant coupling reduction. However, the design complexity of the ADS is quite high.

In this paper, a simple methodology is proposed to reduce the mutual coupling of a dual-polarized and large-scale patch antenna array in a wide band. The technique is to simply mount decoupling dielectric stubs (DDS) that can be fabricated with 3D printing technology on an antenna array seamlessly. By properly optimizing the dielectric constant and dimensions of the dielectric stub, significant mutual coupling reductions can be achieved in a wide band. The presence of the DDS serves as perturbations to slightly localize the electromagnetic fields radiated by one antenna element to weaken the electromagnetic wave coupling in free space or the interface of the substrate and free space. For demonstration, a 4 × 4 dual-polarized and wideband patch antenna array will be implemented with or without DDS. All results are experimentally verified to validate the effectiveness of the proposed decoupling methodology.

The organizations of the paper are as follows: Section II qualitatively explains the decoupling mechanism of the DDS. The dual-polarized and wideband antenna element is presented in Section III. For demonstration, a 4 × 4 dual-polarized decoupled antenna array enabled by the DDS is implemented and parameter studies are carried out in Section IV. The antenna fabrication, measurements, and discussion are given in Section V. Finally, conclusions are summarized in Section VI.

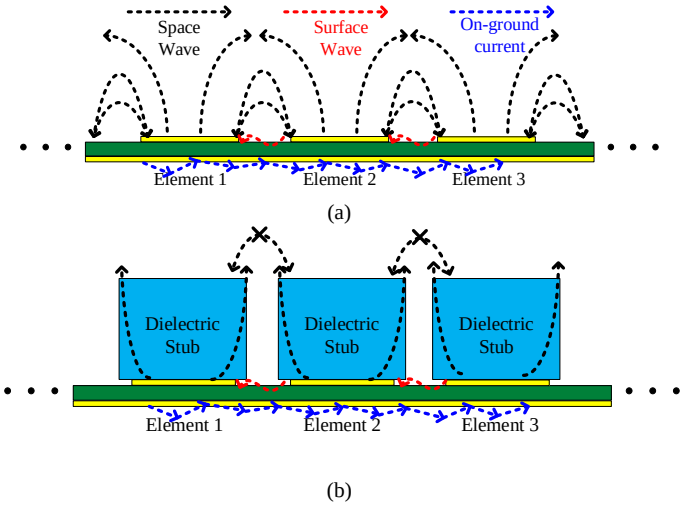

Fig. 2. The schematic diagram of the decoupling methodology. (a). Without the decoupling dielectric stubs (DDS). (b). With the decoupling dielectric stubs (DDS).

II. Decoupling Scheme

The schematic diagrams of an antenna array with and without the proposed DDS are presented in Fig. 2. The decoupling mechanism is qualitatively analyzed from the electromagnetic wave propagation viewpoint. For the antenna array shown in Fig. 2(a), the electromagnetic waves emitting from the antenna element will radiate to free space directly, where the space wave coupling happens between antenna elements. By contrast, the electromagnetic waves will be coupled to the dielectric stub first, and then radiate to free space for the proposed decoupling antenna array shown in Fig. 2(b). As is known, a dielectric material can offer better electromagnetic wave confinement capabilities than air since the permittivity of the dielectric material is higher than that of air. The confinement abilities can perturb the electromagnetic wave propagations, which can be properly employed to reduce the space wave coupling, thereby lowering the mutual couplings between antenna elements.

As the dielectric stub is mounting on the antenna element, the

proposed decoupling scheme should be distinguished from a dielectric resonator antenna. The dielectric constant of a dielectric resonator is usually high (a typical value of 10.2) so that certain operating modes can be excited in the dielectric resonator. However, in the proposed decoupling scheme, the dielectric constant is not allowed to be high: On one hand, the dielectric stub should be avoided to be excited as a dielectric resonator. On the other hand, a low dielectric constant can minimize its impacts on the impedance match of the antenna element so that the dielectric stubs can mount on an antenna array directly for mutual coupling reductions without resizing the antenna element to tune its impedance match.

Compared to the existing techniques for mutual coupling reductions, the proposed methodology is highlighted with the following features:

a). Simple structure: only dielectric constant and dimensions of the dielectric stub need to be optimized to obtain good decoupling performance;

b). Wide decoupling bandwidth: dielectric stubs work at its non-resonant status, so it is wideband;

c). Easy fabrication: no air gap between the antenna array and the DDS, and DDS can be produced by 3D printing technology;

d). Feasible for decoupling of dual-polarized and large-scale (N × N) antenna arrays with improved total efficiency.

III. A Dual-polarized and Wideband Antenna Element

To achieve wideband mutual coupling reductions, a wideband antenna element is essential. Here, the stacking technology is adopted to enable a wideband antenna element [23]-[25]. Fig. 3 presents the geometries of a dual-polarized (+/- 45-degree polarization) and wideband patch antenna element. To broaden the bandwidth of the patch antenna, a parasitic patch is stacked above a driven patch as shown in Fig. 3(a). All supporting substrates are Rogers RO4350B with a dielectric constant of 3.65, a thickness of 1.524 mm, and a loss tangent of 0.0037. Bonding films made of Rogers RO4450F are sandwiched between supporting substrates to connect them tightly, which is characterized by a dielectric constant of 3.52, a thickness of 0.202 mm, and a loss tangent of 0.0029. The dimensions of the patches are properly selected to make the antenna operate at the frequency of interest.

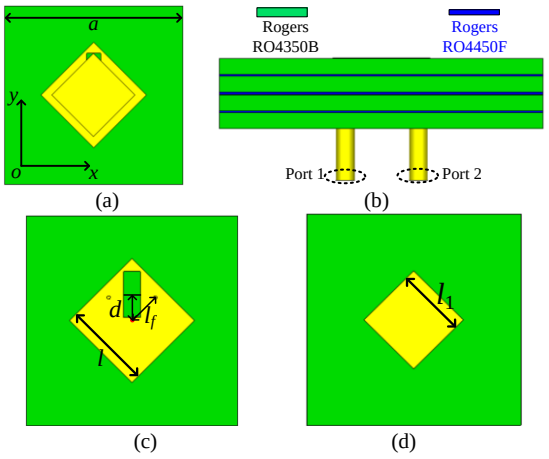

Fig. 3. Geometries of the dual-polarized and wideband stacked patch antenna element. (a). Front view. (b). Side view. (c). Front view of the driven patch. (d). Front view of the parasitic patch. (a = 31 mm, l = 13.5 mm, l_1 = 10.5 mm, l_f = 5.5 mm, d = 1.25 mm, l_s = 2.5 mm, w_s = 0. 7 mm)

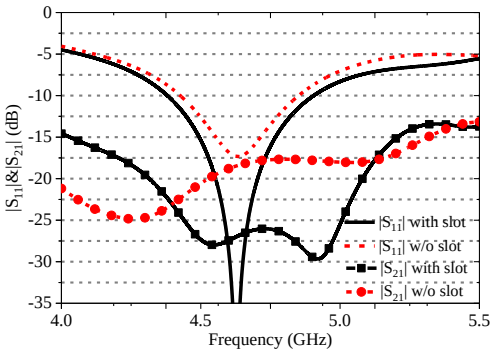

Fig. 4. The simulated S-parameter of the dual-polarized and wideband stacked patch antenna with and without the slot.

For a dual-polarized antenna element, its isolation between the two orthogonal ports is also concerned to fulfill the requirements in MIMO wireless communication systems. Differential feeding technique is effective to achieve high isolation of the two orthogonal ports [26], but it suffers from a relatively bulky volume and a complicated configuration, which is not suitable for large-scale antenna arrays. Here, a slot is etched on the driven patch as shown in Fig. 3(c) to reduce the coupling of the orthogonal ports (ports 1 and 2) and the impedance match of the dual-polarized and wideband antenna element. The slot is characterized by a length of l_s and width of w_s. To verify the effectiveness of the slot, simulations are carried out with our available CST Microwave Studio Software. Fig. 3 compares the S-parameter of the proposed antenna element with and without the slot. As seen in Fig. 4, the coupling between ports 1 and 2 is significantly reduced and the reflection coefficient is better by etching a rectangular slot.

IV. A Decoupled 4 × 4 Dual-Polarized, Wideband Patch Antenna Array

A. Configuration of the proposed 4 × 4 dual-polarized and wideband antenna array with the proposed DDS

Using the proposed antenna element, a 4 × 4 dual-polarized and wideband antenna array with the proposed DDS is performed, dummy elements around the 4 × 4 antenna array are adopted to decrease the edge effects for the outer antenna elements as shown in Fig. 5, and also prove the feasibility for large-scale applications. The DDS is mounting on the antenna array seamlessly without an air gap between the antenna array and DDS as shown in Fig. 5 (c). On the other hand, a massive MIMO antenna array also requires the ability to beamforming at a large scan angle. A small inter-element distance can enlarge the scan angle and avoid the early appearance of the grating lobe at high frequency. Therefore, the inter-element distance is selected as 31 mm, corresponding to 0.485λ at 4.7 GHz. Each antenna port has been numbered to simplify the description as

shown in Fig. 5(a), where the red dot indicates the specific location of the antenna port. The black lines represent the polarizations that the corresponding antenna ports are responsible for.

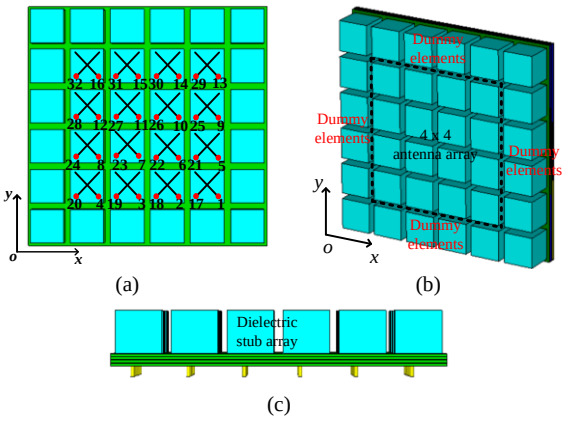

Fig. 5. Initial configurations of the 4 × 4 dual-polarized and wideband antenna array with the DDS. (a). Front view. (b). Perspective view. (c). Side view.

The proposed DDS can be characterized with the following metrics: shape, dielectric constant, height, and side length. Among them, dielectric constant, height, and side length of the dielectric stub play more important roles than its shape in terms of decoupling performance according to the decoupling mechanism described in Sec. II. We have performed some simulations to examine the decoupling performance of the dielectric stub with different specific shapes (e.g. cuboid, cylinder, ellipsoid), where dielectric constant, height and side length are kept the same. It has been observed that all dielectric stubs with different shapes can achieve mutual coupling reductions on different levels. Here, the cuboid dielectric stub with a height of d_h and a side length of d_o is adopted to validate its decoupling performance as it is easiest to fabricate with 3D printing technology. The effects of dielectric constant, height, and side length of the dielectric stub on decoupling performance are studied and simulated with CST software. In the design of a large-scale decoupled antenna array, the mutual couplings between the central antenna element and the remaining antenna elements are usually first checked. Therefore, to simplify the comparison of the decoupling performance, the couplings between antenna port 6 (see Fig. 5 (a)) and the remaining antenna ports are compared under different parameters.

B. Effects of the dielectric constant on decoupling performance

The effects of the dielectric constant of DDS on decoupling performance are examined with the dimensions of the dielectric stub fixed. According to the qualitative analysis of the decoupling mechanism presented in Section II, the dielectric constant of the dielectric stub cannot be high. In order to determine the dielectric constant of the dielectric stub, The S-parameters of the dual-polarized and wideband antenna array with the DDS are simulated and compared with different dielectric constants of 1.5, 2.0, 2.55, 3.0, 3.5, and 4.0. Here, $S_{3,6}$, $S_{6,6}$, $S_{18,6}$, $S_{22,6}$, $S_{23,6}$, $S_{26,6}$ are compared since the remaining mutual couplings are all below -25 dB from 4.4 to 5.0 GHz. As seen in Fig. 6, the mutual couplings are closely related to the dielectric constant of the DDS. A high dielectric constant negatively impacts the impedance match of the antenna element as expected, leading to a worse reflection coefficient ($S_{6,6}$) as observed in Fig. 6(b). As seen in Figs. 6(c), (e), and (f), both a low and a high dielectric constant can cause the mutual couplings of $|S_{18,6}|$, $|S_{23,6}|$, and $|S_{26,6}|$ above -25 dB at some frequencies. When the dielectric constant is 2.55, the mutual couplings can achieve the best levels among other dielectric constants.

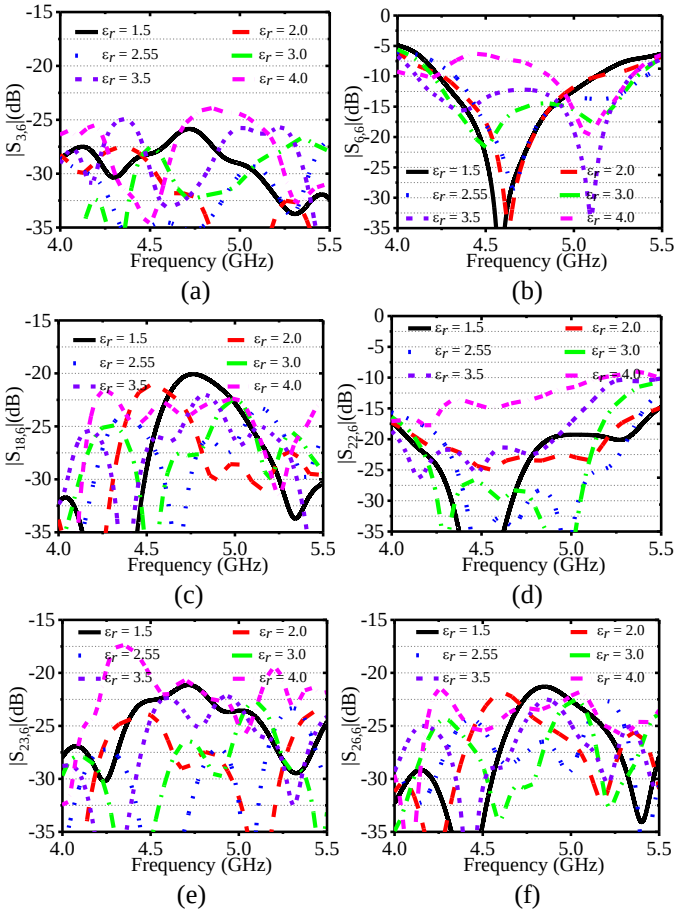

Fig.6. The simulated S-parameters of the dual-polarized and wideband antenna array with different relative permittivity. (a). $|S_{3,6}|$. (b). $|S_{6,6}|$. (c). $|S_{18,6}|$. (d). $|S_{22,6}|$. (e). $|S_{23,6}|$. (f). $|S_{26,6}|$.

The dielectric constant of 2.55 is in line with that of dielectric material for 3D printing. As is known to all, 3D printing technology has become popular in printing dielectric material as it is easy and cheap. In our lab, two available materials are widely used in 3D printing: one is Polylactide (PLA) with a dielectric constant of 2.65, and the other is Acrylonitrile Butadiene Styrene (ABS) with a dielectric constant of 2.55. Here, we choose the ABS material to perform the dielectric stubs, the loss tangent of the ABS material at the millimeter-wave band is around 0.01. It should be mentioned here that other materials with a similar dielectric constant can also be chosen to implement the dielectric stubs.

To further shorten the range of the dielectric constant, a square void is drilled in the center of dielectric stubs to lower its effective dielectric constant since the solid volume of the dielectric stub is reduced, as illustrated in Fig. 7. The side length of the square void is initially set as 5 mm. The S-parameters are simulated with and without the square void. Only the mutual couplings of $S_{7,6}$, $S_{11,6}$, $S_{26,6}$ are compared. As seen in Fig. 8, the presence of the square void can further reduce the mutual couplings. The coupling of $S_{7,6}$ is significantly improved from -22.5 to -25 dB, and the couplings of $S_{11,6}$, $S_{26,6}$ are improved on different levels.

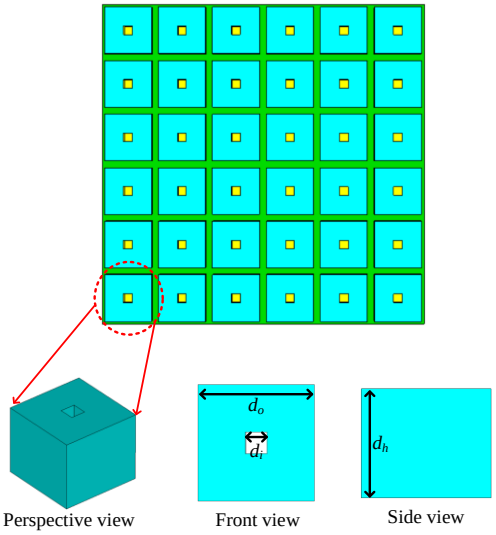

Fig. 7. The updated configuration of the 4 × 4 dual-polarized and wideband patch antenna array with the DDS, where square voids are drilled on the dielectric stubs.

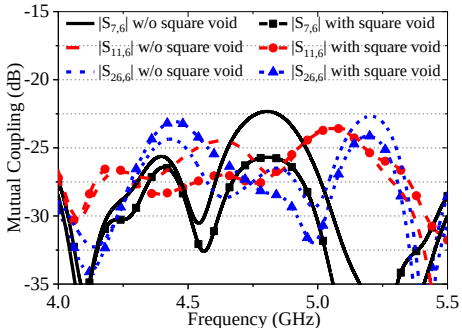

Fig.8. The simulated mutual couplings of the dielectric stub with and without the square void.

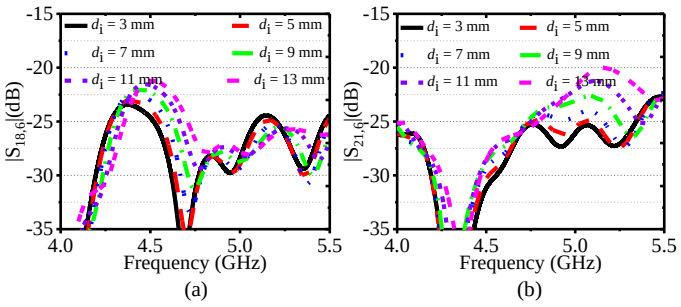

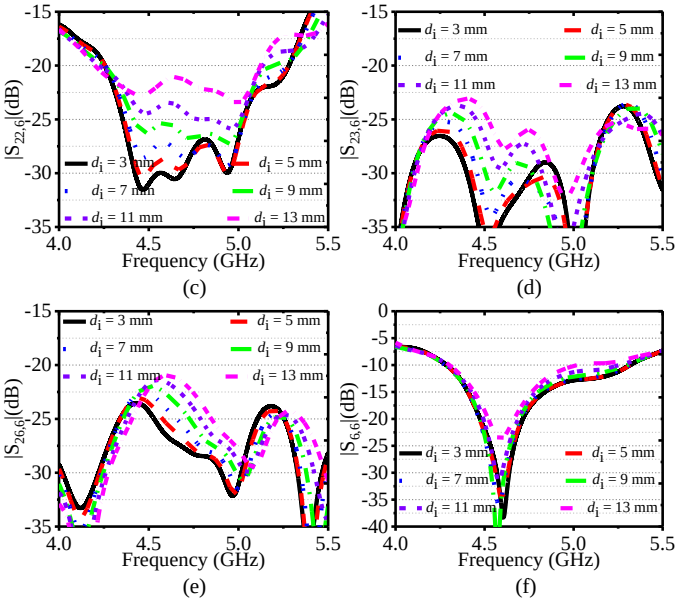

Fig. 9. The simulated mutual couplings of the dual-polarized and wideband antenna array with different values of d_i. (a). $|S_{18,6}|$. (b). $|S_{21,6}|$. (c). $|S_{22,6}|$. (d). $|S_{23,6}|$. (e). $|S_{26,6}|$. (f). $|S_{6,6}|$.

The effects of the side length (d_i) of the square void on decoupling performance are also checked. The S-parameters are simulated and compared with different values of d_i. As seen from Fig. 9, the bandwidth of reflection coefficient of port 6 ($S_{6,6}$) is becoming narrow and the orthogonal mutual coupling ($S_{22,6}$) is getting worse with the increment of d_i. A large d_i equivalently means a low effective dielectric constant of the dielectric stub. The bandwidths of mutual couplings of $S_{18,6}$, $S_{21,6}$, $S_{23,6}$, $S_{26,6}$ below -25 dB are also reduced with the increment of d_i. The results shown in Fig. 9 are also consistent with those from Fig. 6.

C. Effects of the side length on decoupling performance

The effects of the side length (d_o) of the dielectric stub on decoupling performance are studied. As seen in Fig. 10, the reflection coefficient of antenna port 6 can be maintained with different values of d_o. Only the mutual couplings of $S_{11,6}$, $S_{18,6}$, $S_{21,6}$, and $S_{26,6}$ are compared as the remaining mutual couplings are all below -25 dB. As seen in Fig. 10, it is observed that mutual couplings of $S_{11,6}$, $S_{18,6}$, $S_{21,6}$, and $S_{26,6}$ are becoming worse with the increment of d_o. However, a smaller d_o increases the mutual couplings at the low-frequency band on different levels.

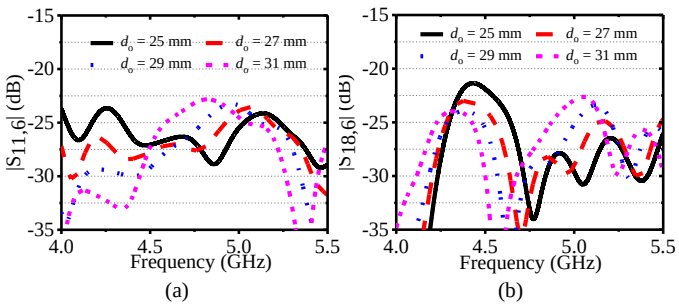

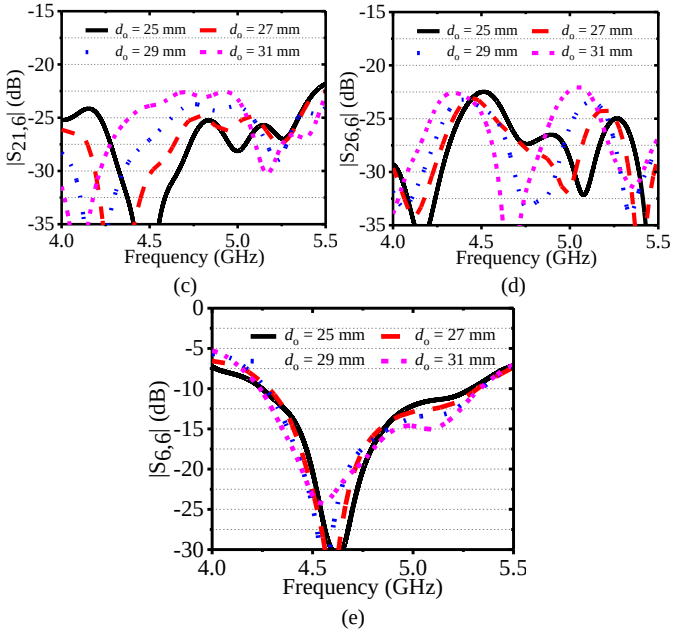

Fig. 10. The simulated mutual couplings of the dual-polarized and wideband antenna array with different values of d_o. (a). $|S_{11,6}|$. (b). $|S_{18,6}|$. (c). $|S_{21,6}|$. (d). $|S_{26,6}|$. (e). $|S_{6,6}|$.

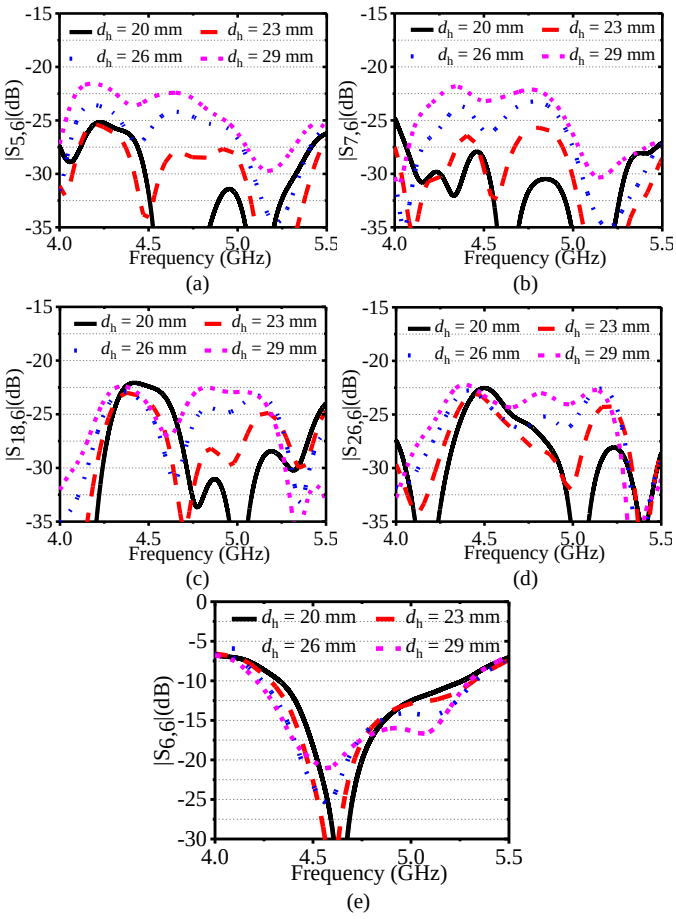

Fig. 11. The simulated mutual couplings of the dual-polarized and wideband antenna array with different values of d_h. (a). $|S_{5,6}|$. (b). $|S_{7,6}|$. (c). $|S_{18,6}|$. (d). $|S_{26,6}|$. (e). $|S_{6,6}|$.

D.Effects of the height on decoupling performance

The height (d_h) of the dielectric sub is varied to check its impact on the decoupling performance. The S-parameters are simulated with different values of d_h. Only the mutual couplings of $S_{5,6}$, $S_{7,6}$, $S_{18,6}$, and $S_{26,6}$ are compared as the remaining mutual couplings are all below -25 dB. As seen in Fig. 11, the mutual couplings of $S_{5,6}$, $S_{7,6}$, $S_{18,6}$, and $S_{26,6}$ are becoming worse with the increment of d_h. A smaller d_h increases the mutual couplings of $S_{18,6}$ and $S_{26,6}$ at the low-frequency band on different levels. From Fig. 11(e), it can be observed that the reflection coefficient of antenna port 6 can still be maintained with different values of d_h. The effects of d_h on the realized gain, total efficiency, and radiation patterns are also examined from simulations. It is found that d_h has negligible impacts on the realized gain, total efficiency, and radiation patterns of the antenna element.

E. Comparison of the decoupling performance

The S-parameters of the dual-polarized and wideband antenna array are simulated with and without the DDS to check the effective decoupling performance of the proposed DDS. The dimensions of the dielectric stub are selected as: d_o = 27mm, d_h = 23mm, d_i = 5mm. Without loss of generality, the mutual couplings of antenna port 1, 17, 6, and 22 in the array with the remaining antenna ports are compared, where the mutual couplings of center and edge antenna ports with the remaining antenna ports in dual-polarization are all considered.

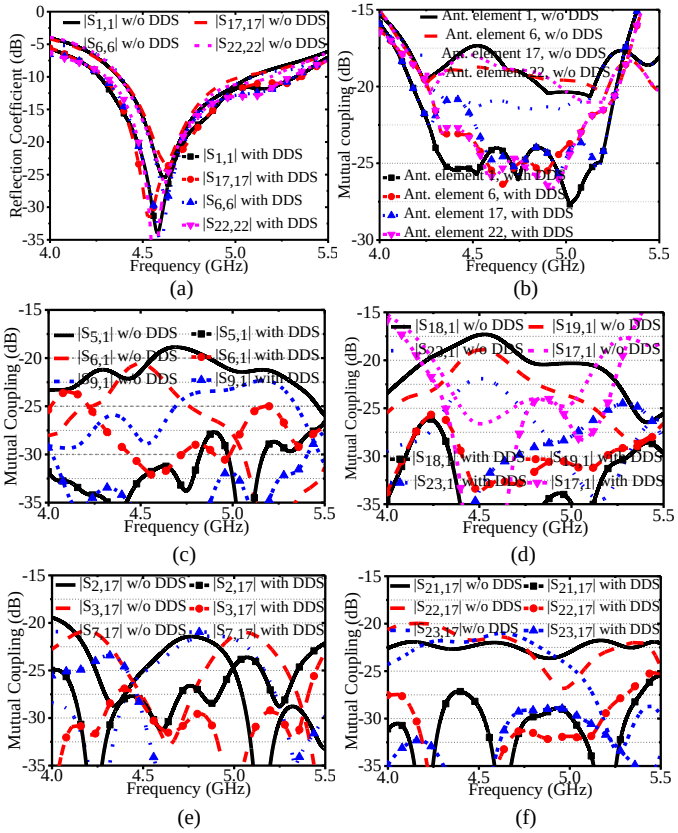

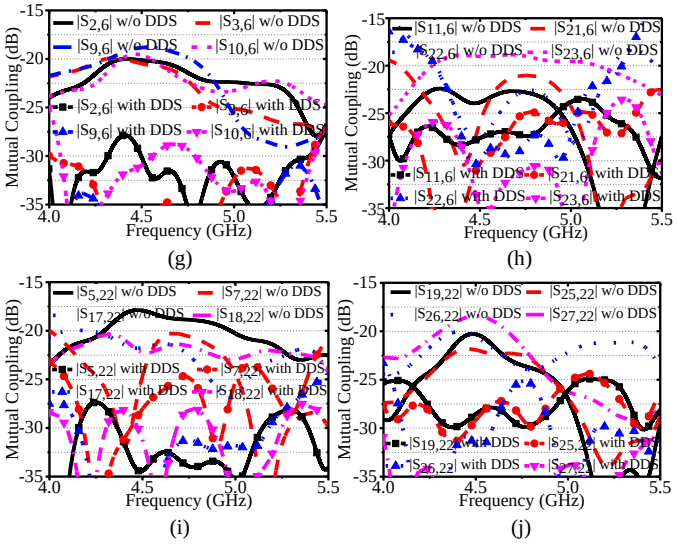

Fig. 12. Comparison of the simulated S-parameters of the dual-polarized and wideband antenna array with and without the DDS. (a). Reflection coefficients of antenna port 1, 17, 6, 22. (b). The mutual coupling envelops of antenna port 1, 6, 17, 22 with and without the DDS. Mutual couplings: (c). between 1 and 5, 6, 9; (d). between 1 and 17, 18, 19, 23; (e). between 17 and 2, 3, 7; (f). between 17 and 21, 22, 23; (g). between 6 and 2, 3, 9, 10; (h). between 6 and 11, 21, 22, 23; (i). between 22 and 5, 7, 17, 18; (j). between 22 and 19, 25, 26, 27.

As seen in Fig. 12 (a), the reflection coefficients of antenna port 1, 6, 17, 22 are not affected by the DDS, the operating bandwidth can still be maintained. The mutual coupling envelops of antenna port 1, 6, 17, 22 that consider all mutual coupling paths are plotted in Fig. 12 (b), where significant mutual coupling reduction is observed. In Figs. 12(c)-(j), the mutual coupling of above -25 dB for the antenna array without DDS is plotted and compared with the one with DDS. For the adjacent antenna port 1 and 5 that have the same polarization, the mutual coupling of S_{51} can be reduced from -18 to -27.5 dB. For the diagonally adjacent antenna ports 1 and 6 having the same polarization, the mutual coupling of S_{61} can be reduced from -20 to -25 dB. For the adjacent antenna ports 1 and 18 that have orthogonal polarizations, the mutual coupling can be reduced from -17.5 to -26 dB. For the antenna port 6 with its (diagonally) adjacent antenna port 2, 3, 9, 10, 11 that possess the same polarization, the mutual couplings of $S_{2,6}$, $S_{3,6}$, $S_{9,6}$, $S_{10,6}$, $S_{11,6}$, are reduced to below -25 dB. For antenna port 6 with its adjacent antenna ports 21 and 23 that have orthogonal polarizations, the mutual coupling of $S_{21,6}$, $S_{23,6}$ can be reduced to below -25 dB.

To further find out the effectiveness and mechanism of the coupling reduction, the current distributions on antenna elements and E-field distributions in the planes of x = 15.5 mm and y = -15.5 mm are plotted at 4.5 GHz when antenna port 6 is excited with the remaining ported terminated with matching loads. As seen in Figs. 13 (a) and (b), the current density on antenna elements with the proposed DDS is much weaker than that without DDS, which sufficiently proves the decoupling performance of the proposed DDS. From the E-field density shown in Figs. 13 (c)-(f), it is observed that the dielectric stub can indeed slightly confine the electromagnetic fields radiating from the antenna element that is excited by antenna port 6. Specifically speaking, the E-field received by antenna port 21 from port 6 without the DDS is stronger than that with the proposed DDS on the plane of y = -15.5 mm at the same zone, while the E-fields that antenna ports 2 and 10 received from the antenna port 6 are stronger than the counterparts with the proposed DDS on the plane of x = 15.5 mm at the same zone, revealing significant mutual coupling reductions. The E-field densities are highly consistent with the mutual coupling of $S_{21,6}$, $S_{2,6}$, $S_{10,6}$ plotted in Figs. 12 (g) and (h).

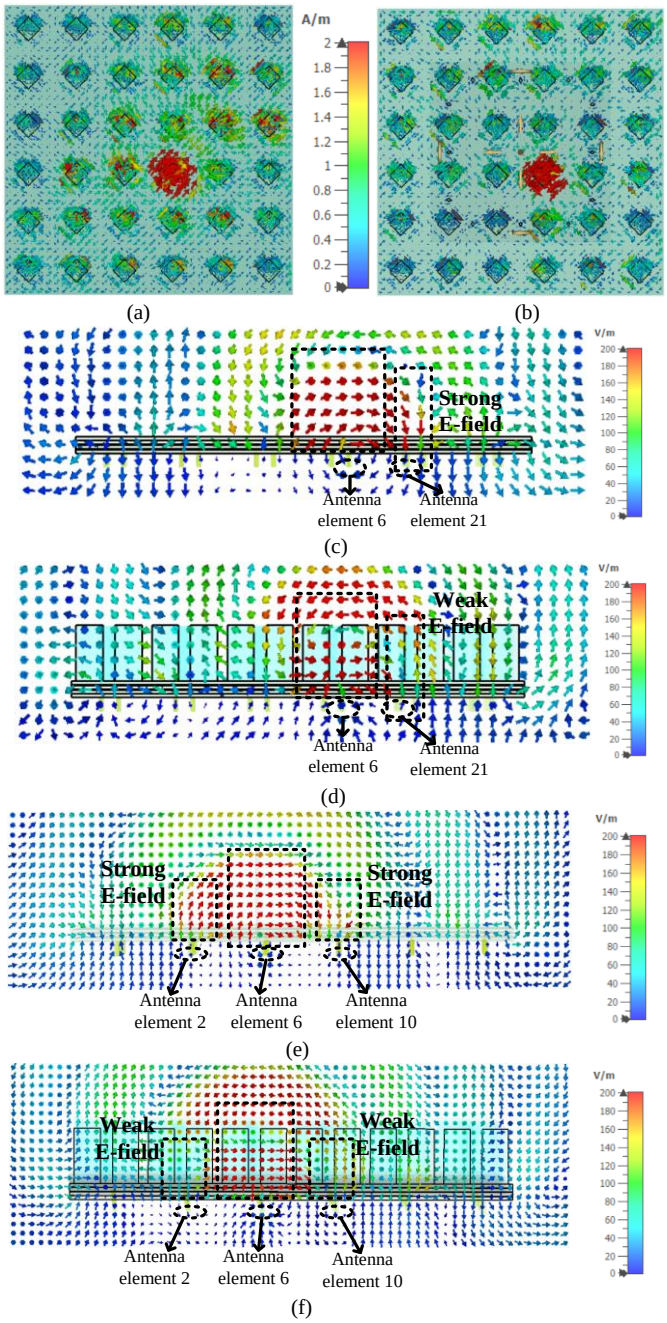

Fig. 13. Simulated current and E-field densities on the antenna arrays when antenna element 6 is excited at 4.5 GHz. Current density: (a). Without the DDS, and (b). With the DDS. E-field density: (c). Without the DDS at y = -15.5 mm, (d). With the DDS at y = -15.5 mm, (e). Without the DDS at x = 15.5 mm, and (f). With the DDS at x = 15.5 mm.

From the current and E-field distributions, it can be observed that the presence of the proposed DDS does not change the operating modes of the antenna array as they have very similar current modes. The dielectric stubs are not excited as the dielectric resonators by the antenna element either.

Based on the analysis above, the design procedures of the DDS for the decoupling of a dual-polarized and wideband antenna array are summarized as follows:

a). design a dual-polarized and wideband antenna element, where dipole antenna or stacked patch antenna is recommended;

b). select a dielectric material with a recommended dielectric constant of around 2.5;

c). optimize the dimensions of the dielectric stub: the height is around 0.3λ to 0.4λ, and the side length is from 0.3λ to 0.5λ. The dimensions of the dielectric stub can be optimized to achieve the desired results; it should be pointed out here the specific shape of the dielectric stub is not unique, the dielectric stub with cylinder, cone, etc., can also achieve decoupling performance on different levels;

V. Measurement and Discussions

In order to validate the effectiveness of the proposed decoupling technique, the antenna arrays with and without DDS have been fabricated and measured. The antenna arrays are produced with multilayer PCB technology. The proposed DDS is printed with our available 3D printer. The photographs of the prototypes are shown in Fig. 14. To attach the DDS on the antenna array firmly, thin cross-shaped dielectric strips and dielectric square ring [as shown in Fig. 14(b)] are printed as well to connect dielectric stubs. Some air holes are drilled on the dielectric strips to align and connect with the antenna array. It should be mentioned here that the thin cross-shaped dielectric strips do not affect the decoupling performance of the DDS.

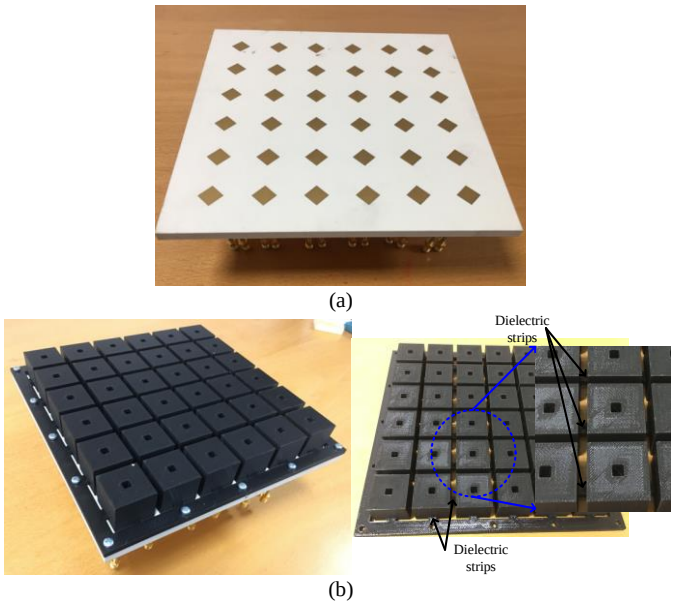

Fig. 14. Photographs of the proposed dual-polarized and wideband antenna arrays. (a). Without the DDS. (b). With the DDS.

A. S-Parameters.

The S-parameters of the proposed dual-polarized and wideband antenna array with and without the DDS are measured and compared. It should be noted that when the mutual coupling of two antenna ports is under test, the other antenna ports are all terminated with matching loads. Here, we select the antenna port of 7, 23, 16, 32 (see Fig. 5 (a)) that are located at the center and edge of the antenna array.

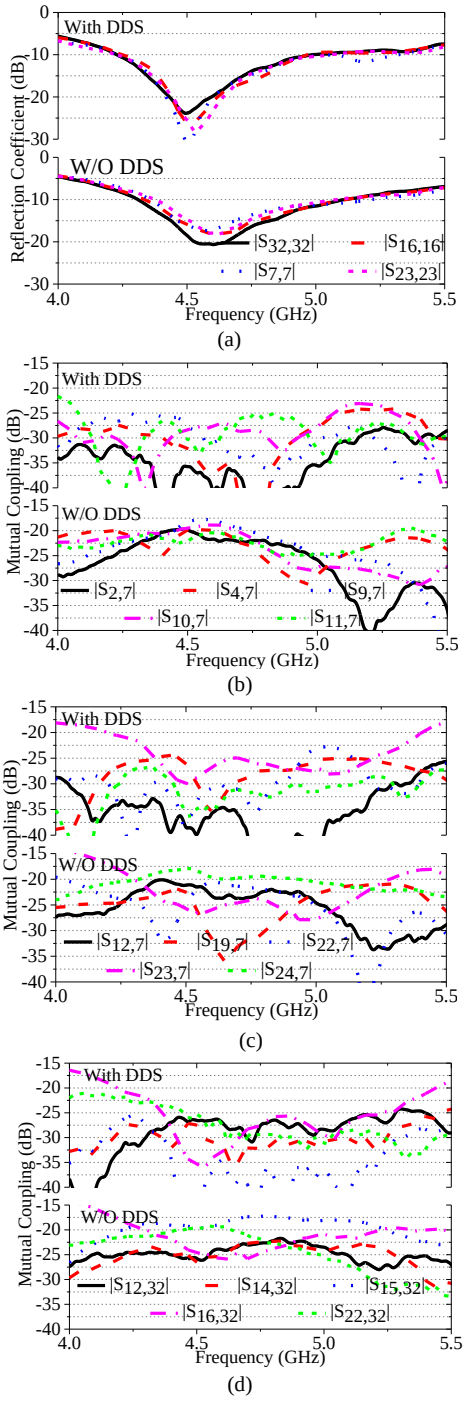

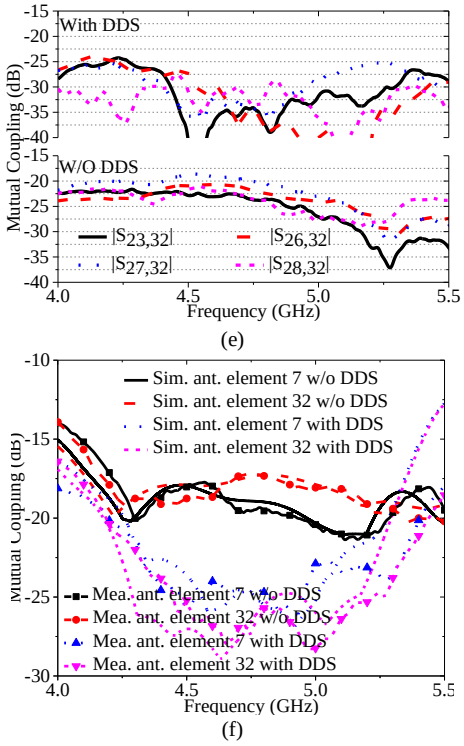

Fig. 15. Measured and simulated S-parameters of the dual-polarized and wideband antenna array with and without the DDS. (a). $|S_{7,7}|$, $|S_{16,16}|$, $|S_{23,23}|$, $|S_{32,32}|$. (b). $|S_{2,7}|$, $|S_{4,7}|$, $|S_{9,7}|$, $|S_{10,7}|$, $|S_{11,7}|$. (c). $|S_{12,7}|$, $|S_{19,7}|$, $|S_{22,7}|$, $|S_{23,7}|$, $|S_{24,7}|$. (d). $|S_{12,32}|$, $|S_{14,32}|$, $|S_{15,32}|$, $|S_{16,32}|$, $|S_{22,32}|$. (e). $|S_{23,32}|$, $|S_{26,32}|$, $|S_{27,32}|$, $|S_{28,32}|$. (f). Measured and simulated mutual coupling envelops of antenna elements 7 and 32.

As seen in Fig. 15 (a), the measured reflection coefficients of antenna port 7, 23, 16, 32 are very close to each other. It also is observed that the presence of the DDS does not affect the reflection coefficients of antenna elements. For mutual coupling comparisons, only $S_{2,7}$, $S_{4,7}$, $S_{9,7}$, $S_{10,7}$, $S_{11,7}$, $S_{12,7}$, $S_{19,7}$, $S_{22,7}$, $S_{23,7}$, $S_{24,7}$, $S_{12,32}$, $S_{14,32}$, $S_{15,32}$, $S_{16,32}$, $S_{22,32}$, $S_{23,32}$, $S_{26,32}$, $S_{27,32}$, $S_{28,32}$ are measured and compared since the remaining mutual coupling are all below -25 dB. As can be seen in Figs. 15 (b) and (c), for the center antenna element, the mutual coupling of $S_{10,7}$ that refers to the diagonal antenna port 7 and 10 having the same polarization is reduced from -18 to -25 dB; the mutual couplings of $S_{22,7}$ that are adjacent antenna port 7 and 22 having the orthogonal polarizations is reduced from -20 to -25 dB. For the edge antenna element, as seen in Figs. 15 (d) and (e), the mutual coupling of $S_{15,32}$ that are adjacent antenna port 15 and 32 having the orthogonal polarization is reduced from -17.5 to -25 dB, the mutual coupling of $S_{27,32}$ that refers to the diagonal antenna port 27 and 32 having the same polarization can be reduced from -18 to -25 dB, the mutual coupling of $S_{28,32}$ that are adjacent antenna port 32 and 28 having the same polarization can be reduced from -21 to -25 dB.

Figs. 15 (b)-(e) demonstrate that the mutual couplings can be reduced to -25 dB from 4.4 to 5.0 GHz, which indicates that the proposed dual-polarized and wideband antenna array with the DDS can achieve all mutual couplings below -25 dB in both co- and cross-polarization. Fig. 15 (f) compares the measured and simulated mutual coupling envelops (that include the worst coupling from all the curves/paths) of antenna ports 7 and 32. It is observed that the simulated and measured results are consistent, the measured mutual coupling envelop is below -25 dB from 4.4 to 5.0 GHz.

B. Radiation patterns, realized gains, and total efficiencies

The radiation patterns, realized gains, and total efficiencies of the dual-polarized and wideband antenna array with and without the DDS have been measured and compared when antenna port 7, 23, 6, 22, 16, 23 is excited respectively in our anechoic chamber, where the antenna element with ports 7 and 23 is adjacent to the antenna element with ports 6 and 22. It should be mentioned here when one antenna port is excited the remaining antenna ports are terminated with the matching loads.

Fig. 15 compares the measured normalized radiation patterns of the dual-polarized and wideband antenna array with and without the DDS at 4.5 GHz. As seen in Fig. 16, the measured co-polarizations (co-pol) have great agreements from -60 and +60 degrees in both horizontal and vertical planes, which indicates the presence of the DDS would not significantly affect the radiation patterns of the antenna element. Besides, it is also observed that the radiation patterns are stable from -60 to +60 degrees when antenna port 7, 23, 6, 22, 16, 32 are excited respectively. The measured cross-polarization (cro-pol) levels are better than -8.0 dB from -60 to 60 degrees in both horizontal and vertical planes, especially better than -10 dB at broadside when antenna port 7, 23, 6, 22, 16, 32 is excited respectively.

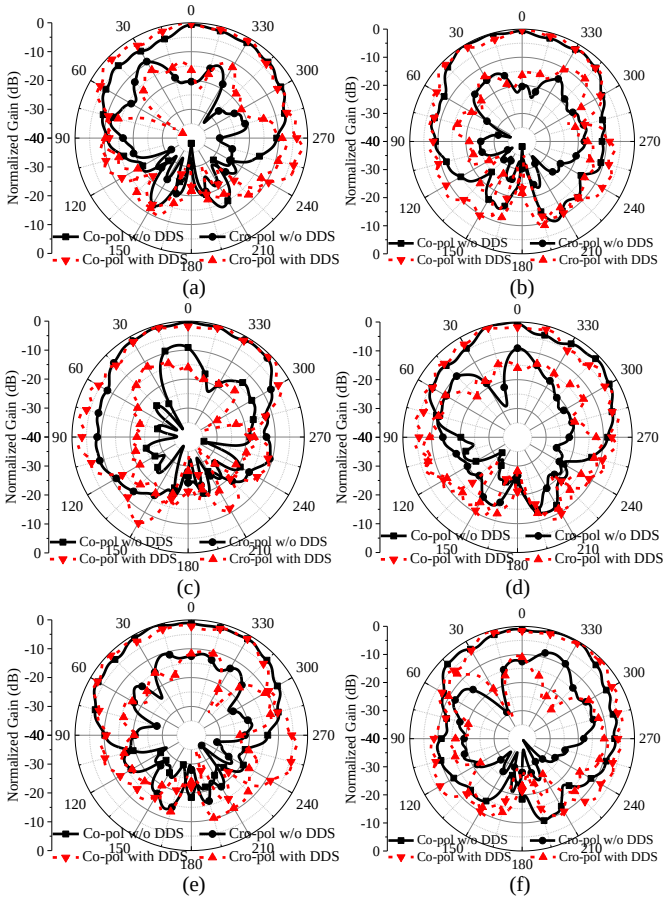

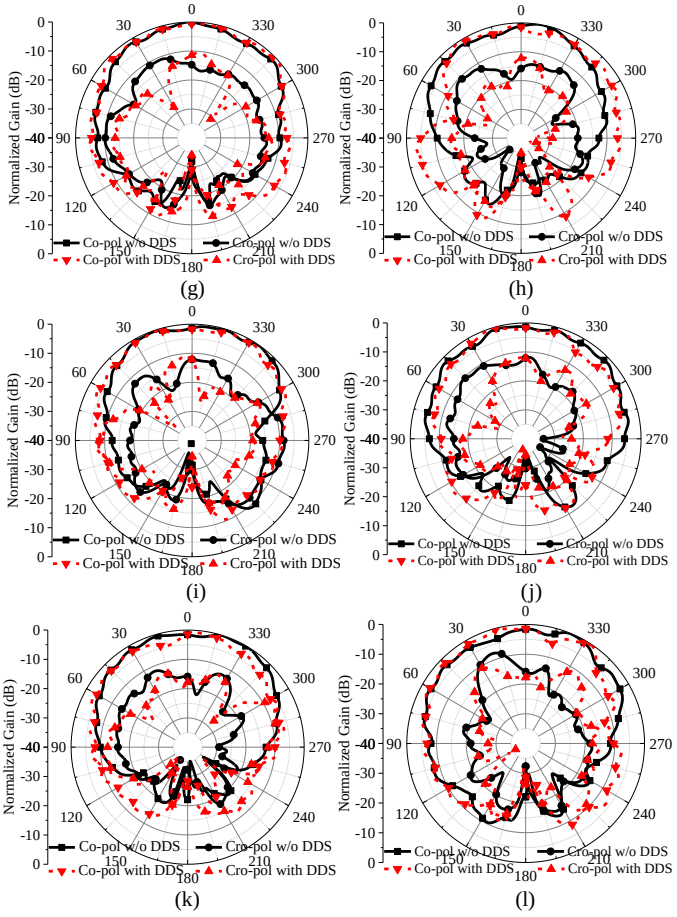

Fig. 16. Measured normalized radiation patterns of the dual-polarized and wideband antenna array with and without the DDS. (a). Horizontal plane with antenna port 7 excited. (b). Vertical plane with antenna port 7 excited. (c). Horizontal plane with antenna port 23 excited. (d). vertical plane with antenna port 23 excited. (e). vertical plane with antenna port 6 excited. (f). vertical plane with antenna port 6 excited. (g). vertical plane with antenna port 22 excited. (h). vertical plane with antenna port 22 excited. (i). vertical plane with antenna port 16 excited. (j). vertical plane with antenna port 16 excited. (k). vertical plane with antenna port 32 excited. (l). vertical plane with antenna port 32 excited.

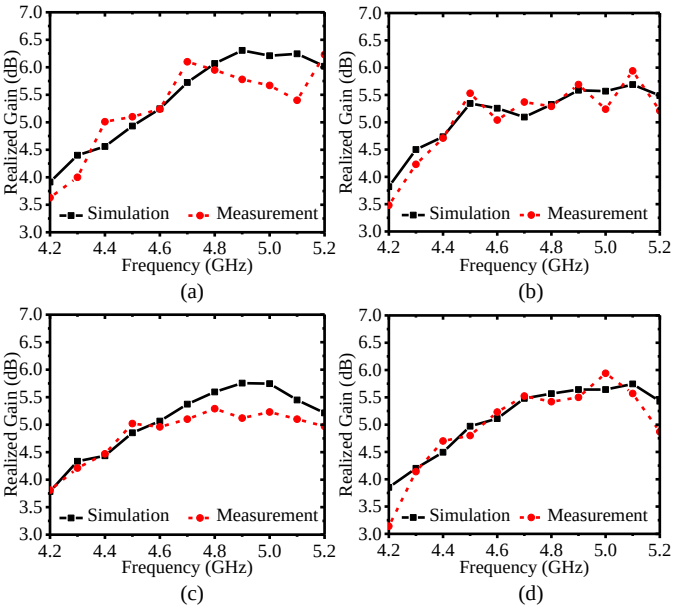

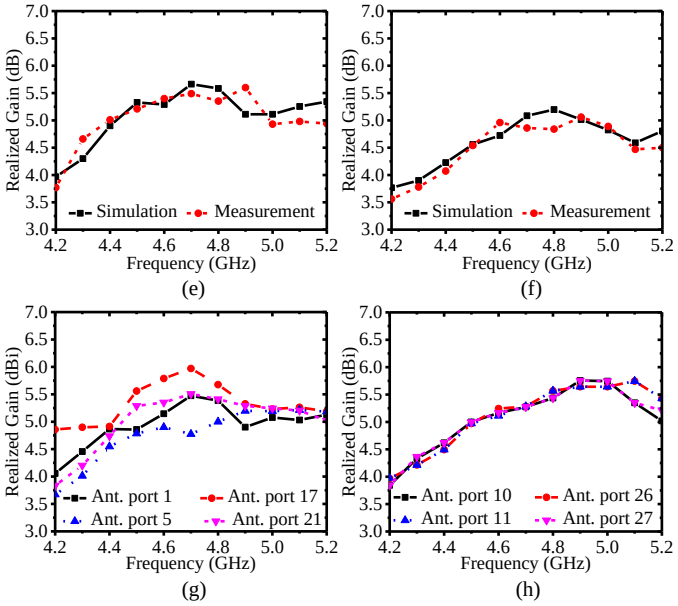

Fig. 17. Measured and simulated realized gains of antenna elements with the DDS. (a). Antenna port 7. (b). Antenna port 23. (c). Antenna port 6. (d). Antenna port 22. (e). Antenna port 16. (f). Antenna port 32. (g). Simulated realized gains when antenna port 1, 17, 5, 21 is excited respectively. (h). Simulated realized gains when antenna port 10, 26, 11, 27 is excited respectively.

The realized gains of the dual-polarized and wideband antenna array with the DDS are measured and compared with the simulated results when antenna port 7, 23, 6, 22, 16, 32 are excited respectively. As seen in Fig. 17, the measured realized gains range from 3.5 to 6.2 dBi from 4.4 to 5.0 GHz. The measured and simulated results are close to each other with a gain difference of less than 0.7 dB. We also provide the simulated realized gain with frequencies when antenna port 1, 17, 5, 21, 10, 26, 11, 27 is excited respectively as shown in Figs. 17 (g) and (h). The total efficiencies of antenna elements from the proposed antenna array with and without the DDS are measured and compared. As seen in Fig. 18, the simulated total efficiencies with the presence of the DDS are higher than the counterparts without the DDS when antenna port 7, 23, 6, 22, 16, 32 is excited respectively, which is one of the advantages of the proposed DDS method. The measured results are also plotted in Fig. 18 for comparison, which aligns very well with the simulated results. The higher total efficiencies might be explained by the electric field distributions shown in Fig. 13. The DDS can slightly localize the electromagnetic fields, reducing the loss introduced by the electromagnetic wave propagation on the surface of the antenna array.

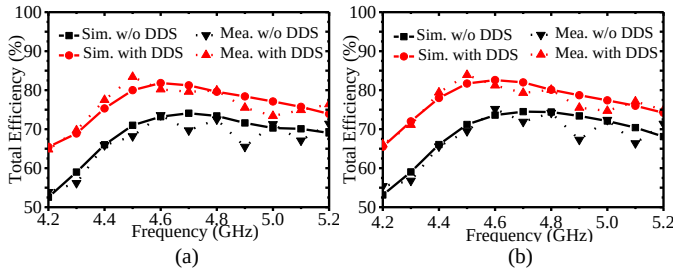

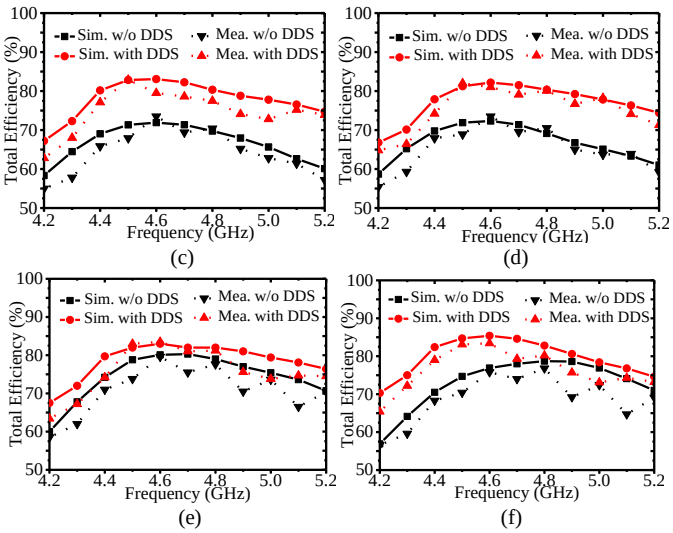

Fig. 18. Measured and simulated total efficiencies of the antenna elements. (a). Antenna element 7. (b). Antenna element 23. (c). Antenna element 6. (d). Antenna element 22. (e). Antenna element 16. (f). Antenna element 32.

C. Performance comparisons with the previous state-of-the-art work.

The performance of the proposed DDS for the decoupling of a dual-polarized and wideband antenna array is compared with other related and state-of-the-art work.

As seen in Tab. I, the proposed DDS can achieve below -25 dB mutual couplings for antenna elements with the smallest inter-element distance in the lowest complexity configuration. The bandwidth of the proposed antenna array with the mutual coupling below -25 dB is 12.8%, which is much wider than the results in [17], [20], and is comparable with the bandwidth in [21] and [22]. Since the height of the dielectric stub is closely related to the decoupling performance of the proposed DDS, the profile of the proposed decoupling method is indeed higher than that in [17] and [20], but is comparable with the height in [21], [22] that an air separation between the ADS and the metal ground is needed. Compared to the technique of ADS, the proposed DDS can mount on the antenna array without any air gap, which simplifies and facilitates the assembling of the entire antenna. As the gains of antenna elements are closely associated with their specific structures, they are different from each other. The gain of the antenna element with the proposed DDS is comparable with the results in [17], [22], but is smaller than that in [20], [21]. The total efficiencies of the antenna elements in the proposed decoupling method are slightly smaller than those in [20], which is mainly attributed to the specific structure of the antenna element. But the total efficiencies of antenna elements in the antenna array have been improved by around 10% after adding the proposed DDS, which is a remarkable highlight compared with [17], [20]-[22].

Regarding the cross-polarization levels, the measured cross-polarizations of multiple antenna elements have been presented in our and the referred work. Here, the worst cross-polarization level in both horizontal and vertical planes from -60 to +60 degrees is compared, where a comparable cross-polarization level is observed among the proposed decoupling method and other work. The slightly higher cross-polarization is closely associated with< the specific structure of the antenna element but has nothing to do with the proposed DDS. In our proposed antenna element [as shown in Fig. 3], a rectangular slot is etched on the patch to improve the isolation of the two orthogonal ports (e.g. port *i* and *i* + 16) but it strengthens the cross-polarization level.

Tab. I. Performance comparison of the proposed design with other related work.

Ref	Imp. BW (GHz)	Array distance & Height	Gain (dBi)	Scale	BW with **decoupling < -25 dB**	Total efficiency	Cross-pol (dB)	Pol.	Decoupling technique	Complex.	Feasible for N x N antenna array
[17]	4.8-5.0	0.50 λ_0 x 0.50 λ_0 & 0.274λ_0 (λ_0@4.9GHz)	5.3	4 × 4	4.85-4.95 (2.0%)	> 70%	> 10.0	0/90 degrees	Decoupling network	High	Yes
[20]	4.7-5.2	0.62 λ_0 & 0.25λ_0 (λ_0@4.9GHz)	7.3	4 × 4	4.9-5.2 (6.1%)	> 90%	> 10.0	0/90 degrees	DG	High	Yes
[21]	3.2-3.9	0.53 λ_0 x 0.71 λ_0 & 0.33λ_0 (λ_0@3.55GHz)	8.0	2 × 2	3.3-3.8 (14.1%)	–	> 10.0	+/-45 degrees	ADS	High	Unknown
[22]	3.2-3.9	0.65 λ_0 & 0.40λ_0 (inter-element) (λ_0@3.55GHz)	6.0	4 × 4	3.3-3.8 (14.1%)	–	> 10.0	+/-45 degrees	ADS	High	Yes
Pro.	**4.25-5.25**	**0.485λ_0 x 0.485λ_0 & 0.466λ_0 (λ_0@4.7GHz)**	**5.7**	**4 × 4**	**4.4-5.0 (12.8%)**	**> 76%**	> 8.0	**+/-45 degrees**	**DDS**	**Low**	**Yes**

VI. Conclusions

This paper introduced a simple and effective methodology for the decoupling of a dual-polarized, wideband, and large-scale antenna array by mounting a DDS on the array. The presence of DDS is considered as electromagnetic perturbations to slightly localize the electromagnetic field radiating from the antenna element to suppress the inter-element mutual coupling. The dielectric constant of the DDS is preferred to be low to obtain optimal decoupling performance and small impact on array element impedance match. The DDS can achieve good isolation by optimizing its dimensions. A 4 × 4 dual-polarized and wideband antenna array with the proposed DDS has been designed, fabricated, and measured for demonstration. The results uncover that the proposed DDS can achieve mutual couplings of below -25 dB from 4.4 to 5.0 GHz in both co- and cross-polarization without significantly changing antenna radiation patterns. Furthermore, the total efficiencies of antenna elements are also improved.

Acknowledgements

The authors would like to thank the lab engineer Ben Krøyer for his help in soldering the connectors for the prototype, Kim Olesen for his kind assistance in the measurement setup.

References

[1] R. He, B. Ai, G. Stuber, G. Wang, and Z. Zhong, "Geometrical based modeling for millimeter wave MIMO mobile-to-mobile channels," *IEEE Trans. Veh. Technol.*, vol. 67, no. 4, pp. 2828–2863, Apr 2018.

[2] T. S. Rappaport, S. Sun, R. Mayzus, H. Zhao, Y. Azar, K. Wang, G. N. Wong, J. K. Schulz, M. Samimi, and F. Gutierrez, "Millimeter wave mobile communications for 5G cellular: It will work!" *IEEE Access*, vol. 1, pp. 335-349, 2013.

[3] Y. Xin, D. Wang, J. Li, H. Zhu, J. Wang, and X. You, "Area spectral efficiency and area energy efficiency of massive MIMO cellular systems," *IEEE Trans. Veh. Technol.*, vol. 65, no. 5, pp. 3243–3254, May 2016.

[4] E. G. Larsson, O. Edfors, F. Tufvesson, and T. L. Marzetta, ''Massive MIMO for next generation wireless systems,'' *IEEE Communication Magazine*, vol. 52, no. 2, pp. 186-195, Feb. 2014.

[5] X. Chen, S. Zhang, and Q. Li, "A review of mutual coupling in MIMO systems." *IEEE Access*, vol. 6, pp. 24706-24719, 2018.

[6] S. Hwangbo, H. Yang, and Y. Yoon, "Mutual coupling reduction using micromachined complementary meander-line slots for a patch array antenna," *IEEE Antennas Wireless Propag. Lett*, vol. 16, pp. 1667-1670, 2017.

[7] J. Ouyang, F. Yang, and Z. M. Wang, "Reducing mutual coupling of closely spaced microstrip MIMO antennas for WLAN application," *IEEE Antennas Wireless Propag. Lett.*, vol. 10, pp. 310-313, 2011.

[8] K. Wei, J. Li, L. Wang, Z. Xing, and R. Xu, "Mutual coupling reduction by novel fractal defected ground structure bandgap filter," *IEEE Trans. Antennas Propag*., vol. 64, no. 10, pp. 4328-4335, Oct. 2016.

[9] W. Wang, Z. Zhao, Q. Sun, X. Liao, Z. Fang, K. See, and Y. Zheng, "Compact quad-element vertically-polarized high-isolation wideband MIMO antenna for vehicular base station," *IEEE Trans. Veh. Technol.*, vol. 69, no. 9, pp. 10000–10008, Sept 2020.

[10] F. Yang, and Y. Rahmat-Samii, "Microstrip antennas integrated with electromagnetic band-gap (EBG) structures: A low mutual coupling design for array applications," *IEEE Trans. Antennas Propag*., vol. 51, no. 10, pp. 2936-2946, Oct. 2003.

[11] M. Gulam Nabi Alsath, M. Kanagasabai, and B. Balasubramanian, "Implementation of slotted meander-line resonators for isolation enhancement in microstrip patch antenna arrays," *IEEE Antennas Wireless Propag. Lett.*, vol. 12, pp. 15-18, 2013.

[12] H. Farahani, M. Veysi, M. Kamyab, and A. Tadjalli, "Mutual coupling reduction in patch antenna array using a UC-EBG superstrate," *IEEE Antennas Wireless Propag. Lett.*, vol. 9, pp. 57-59, 2010.

[13] J. Lee, S. Kim, and J. Jang, "Reduction of mutual coupling in planar multiple antenna by using 1-D EBG and SRR structures," *IEEE Trans. Antennas Propag*., vol. 8, no. 15, pp. 1261-1267, Sep. 2015.

[14] M. Li, L. Jiang, and K. Yeung, "A general and systematic method to design neutralization lines for isolation enhancement in MIMO antenna arrays," *IEEE Trans. Veh. Technol.*, vol. 69, no. 6, pp. 6242–6253, June 2020.

[15] S. Zhang, and G. F. Pedersen, "Mutual coupling reduction for UWB MIMO antennas with a wideband neutralization line," *IEEE Antennas Wireless Propag. Lett.*, vol. 15, pp. 166-169, 2016.

[16] S. Su, C. Lee, and F. Chang, "Printed MIMO-antenna system using neutralization-line technique for wireless USB-dongle applications," *IEEE Trans. Antennas Propag*., vol. 60, no. 2, pp. 456-463, Feb. 2012.

[17] Y.-M. Zhang, S. Zhang, J.-L. Li, and G. F. Pedersen, "A transmission-line-based decoupling method for MIMO antenna arrays," *IEEE Trans. Antennas Propag*., vol. 67, no. 5, pp. 3117-3131, May 2019.

[18] Y.-M. Zhang, S. Zhang, J.-L. Li, and G. F. Pedersen, "A Wavetrap-Based Decoupling Technique for 45°-Polarized MIMO Antenna Arrays," *IEEE Trans. Antennas Propag*., vol. 68, no. 3, pp. 2148-2157, Mar. 2020.

[19] M. Lin, and S. Cheung, "A novel calculation-based parasitic decoupling technique for increasing isolation in multiple-element MIMO antenna arrays," *IEEE Trans. Veh. Technol.*, vol. 70, no. 1, pp. 446–458, Jan 2021.

[20] S. Zhang, X. Chen, and G. F. Pedersen, "Mutual coupling suppression with decoupling ground for massive MIMO antenna arrays," *IEEE Trans. Veh. Technol.*, vol. 68, no. 8, pp. 7273–7282, Aug 2019.

[21] K. Wu, C. Wei, X. Mei, and Z. Zhang, "Array-antenna decoupling surface," *IEEE Trans. Antennas Propag.*, vol. 65, no. 12, pp. 6728–6738, Dec. 2017.

[22] C. Wei, Z. Zhang, and K. Wu, "Phase compensation for decoupling of large-scale staggered dual-polarized dipole array antennas," *IEEE Trans. Antennas Propag.*, vol. 68, no. 4, pp. 2822–2831, Apr. 2020.

[23] A. Serra, P. Nepa, G. Manara, G. Tribellini, and S. Cioci, "A wide-band daul-polarized stacked patch antenna," *IEEE Antennas Wireless Propag. Lett*, vol. 6, pp. 141-143, 2007.

[24] M. Matin, B. Sharif, and C. Tsimenidis, "Probe fed stacked patch antenna for wideband applications," *IEEE Trans. Antennas Propag.*, vol. 55, no. 8, pp. 2385–2388, Aug. 2007.

[25] W. Yang, J. Zhou, Z. Yu, and L. Li, "Single-fed low profile broadband circularly polarized stacked patch antenna," *IEEE Trans. Antennas Propag.*, vol. 62, no. 10, pp. 5406–5410, Oct. 2014.

[26] Y. Liu, S. Wang, X. Wang, and Y. Jia, "A differentially fed dual-polarized slot antenna with high isolation and low profile for base station application," *IEEE Antennas Wireless Propag. Lett*, vol. 18, no. 2, pp. 303-307, Feb. 2019.